ELEKTROTEHNIŠKI VESTNIK 93(1-2): 44–55, 2026
ORIGINAL SCIENTIFIC PAPER

EKF-Based Target Estimation for the APN Missile Guidance Using a YOLO-Driven Seeker

Mirza Hodžić, Naser Prljača

Department of Control Systems and Robotics, University of Tuzla, Tuzla, Bosnia and Herzegovina

Abstract. Modern tactical missile guidance laws require an accurate target tracking and state estimation to effectively intercept maneuvering targets. The Proportional Navigation (PN) is one of the most widely used guidance laws for tactical missiles, relying on line-of-sight (LOS) rate measurements to generate lateral acceleration commands. Missiles typically employ electro-optical or infrared seekers. Our study utilizes a two-axis gimbaled camera seeker which employs a laser range finder, equipped with the YOLO algorithm for a real-time target detection tracking and recognition. The seeker provides the image acquisition, target detection, tracking, and LOS rate measurement relative to the inertial frame. Additionally, an Extended Kalman Filter (EKF) is used to filter the LOS rate measurements and to estimate the target three-dimensional motion, as well as lateral accelerations. The estimates are then used to implement the Augmented Proportional Navigation (APN) which reduces the required missile lateral acceleration compared to the standard PN guidance. The study findings are validated using a six-degrees-of-freedom (6-DOF) nonlinear missile model, demonstrating its effectiveness when integrating the deep-learning-based target tracking with the modern guidance laws.

Keywords: EKF, Missile guidance, YOLO, 6DOF, APN, Seeker.

Ocenjevanje cilja z razširjenim Kalmanovim filtrom za vodenje rakete APN z uporabo iskalnika YOLO

Sodobni zakoni vodenja taktičnih raket zahtevajo natančno sledenje cilju in ocenjevanje njegovega stanja za učinkovito prestrezanje manevrirajočih ciljev. Proporcionalna navigacija je eden najpogosteje uporabljenih zakonov vodenja, ki temelji na meritvah hitrosti spremembe smerne črte za generiranje bočnih pospeškov. Rakete običajno uporabljajo elektrooptične ali infrardeče iskalnike. V naši raziskavi uporabljamo dvoosni kardaniziran kamerni iskalnik z laserskim merilnikom razdalje, opremljen z algoritmom YOLO za zaznavanje, sledenje in prepoznavanje ciljev v realnem času. Iskalnik omogoča zajem slike, zaznavanje cilja, sledenje ter merjenje hitrosti spremembe smerne črte glede na inercialni koordinatni sistem. Poleg tega uporabljamo razširjeni Kalmanov filter za filtriranje meritev in oceno tridimenzionalnega gibanja cilja ter bočnih pospeškov. Te ocene nato uporabimo pri razširjeni proporcionalni navigaciji, ki v primerjavi s standardno zmanjša potrebne bočne pospeške rakete. Rezultati raziskave so potrjeni z nelinearnim modelom rakete s šestimi stopnjami prostosti in kažejo učinkovitost povezovanja sledenja cilju na osnovi globokega učenja s sodobnimi zakoni vodenja.

1 INTRODUCTION

Proportional navigation(PN) is the most widely used guidance law for tactical missiles relying on the line-of-sight (LOS) rate measurements to generate lateral acceleration commands. The main PN idea of proportional navigation is to generate commanded accelerations normal to the instantaneous LOS to the target [1]–[4]. The PN guidance requires measurements of the LOS rate and the closing velocity. The generated acceleration commands are provided to the autopilot as setpoint values.

The missile autopilots range from classical linear designs to advanced nonlinear controllers [5]–[8]. Our study considers a linear autopilot that stabilizes the roll channel to allow an independent control of the pitch and yaw, where lateral accelerations are realized through cascade PID controllers with inner damping loops.

The LOS rate measurements are provided by the seeker subsystem which incorporates a two-axis gimbaled camera capable of an independent pitch and yaw motion. The target detection and tracking are performed using the YOLO algorithm [9] with the image-plane coordinates converted into tracking errors to drive the seeker stabilization. An accurate LOS rate estimation is then achieved by combining the seeker gimbal angular rates, tracking errors, and missile body rates. In [10], the author implements a similar seeker system for a PN-guided missile without state estimation.

Since the image-based measurements obtained from the YOLO detector are inherently noisy, the LOS rates must be filtered prior to the guidance law implementation. An Extended Kalman Filter (EKF) is employed both to filter the LOS measurements and to estimate the target kinematics, including the lateral accelerations.

Received 28 February 2026
Accepted 18 March 2026

These estimates enable an Augmented Proportional Navigation (APN) which reduces the missile maneuvering requirements compared to the standard PN guidance law. Previous studies [11]–[15] apply EKF for APN, but are limited to two-dimensional scenarios. A [16] reports three-dimensional implementation with no estimation of the target accelerations normal to the velocity vector and no seeker implementation. Recent [17] implements EKF for the LOS rate estimation from a relative displacement between the seeker gimbals and strapdown inertial measurement unit without using any image acquisition and machine learning for target tracking.

Our study contributes to the development of a three-dimensional EKF-based target tracking framework integrated with the PN and APN guidance laws on a 6-DOF nonlinear missile model. Our system incorporates a two-axis gimbaled seeker camera with a YOLO-based target tracking, providing a unified approach that advances both the guidance law performance and the seeker implementation.

Section II of our study introduces a 6-DOF model to simulate the guidance law, the estimator and the seeker. Section III describes the actuator model. Section IV explains the autopilot subsystem. Section V covers PN and APN and compares them. Section VI explains the YOLO deep learning neural network used to localize the target. Section VII covers the camera module and explains how the tracking errors are obtained from the image. Section VIII covers the seeker system and shows how the LOS rate can be reconstructed. Section IX covers EKF, explaining the model used for the filter implementation. Section X covers the synthesis and implementation of the guidance system. Finally, Section XI presents two simulation scenarios, showing the usefulness of the presented system and explaining the benefits of the APN guidance.

2 MISSILE 6DOF MODEL

In order to accurately simulate the missile guidance, a feasible dynamic missile 6DOF model is used. The missile motion can be described by six nonlinear coupled first-order differential equations [18]–[24]:

$$\dot{P} = L/I_x \tag{1}$$

$$\dot{Q} = PR\left(I_z - I_x\right)/I_y + M/I_y \tag{2}$$

$$\dot{R} = PQ\left(I_x - I_y\right)/I_z + N/I_z \tag{3}$$

$$\dot{u} = vR - wQ + F_x/m \tag{4}$$

$$\dot{v} = wp - uR + F_y/m \tag{5}$$

$$\dot{w} = uQ - vP + F_z/m \tag{6}$$

where u, v, and w are the missile velocities along the x, y, and z axes of the missile body frame. P, Q and R are the rotational angular velocities about the x, y and z axes of the missile body frame. L, M and N are are the moments acting along the x, y and z axes of the missile body frame. F_x, F_y and F_z are the total forces acting along the missile body axes. Forces acting along the missile body are the thrust, gravitational and aerodynamic forces and they have to be transformed into the body frame. The gravitational force is naturally given in the inertial frame as $G = \begin{bmatrix}0 & 0 & mg\end{bmatrix}^T$ and can be transformed as $T_B^E G$, where T_B^E is given as [25]:

$$T_B^E = \begin{bmatrix} c\theta c\psi & c\theta s\psi & -s\theta \\ s\phi s\theta c\psi - c\phi s\psi & s\phi s\theta s\psi + c\phi c\psi & s\phi c\theta \\ c\phi s\theta c\psi + s\phi s\psi & c\phi s\theta s\psi - s\phi c\psi & c\phi c\theta \end{bmatrix} \tag{7}$$

Now, the total forces acting along the missile body are calculated as:

$$\begin{bmatrix} F_x \\ F_y \\ F_z \end{bmatrix} = \begin{bmatrix} T \\ 0 \\ 0 \end{bmatrix} + mg \begin{bmatrix} -\sin\theta \\ \sin\phi\cos\theta \\ \cos\phi\cos\theta \end{bmatrix} + \begin{bmatrix} F_{Ax} \\ F_{Ay} \\ F_{Az} \end{bmatrix} \tag{8}$$

where T is the thrust force, g is the gravitational acceleration and m is the mass of the missile, assumed to be constant. Angles θ, ϕ and ψ are the Euler RPY angles which describe orientation in reference to the fixed inertial reference frame. Forces F_{Ax}, F_{Ay} and F_{Az} are the aerodynamic forces acting along the missile body axis. They are highly nonlinear functions depending on all the state variables and mostly upon the Mach number, angle of the attack α and sideslip angle β. The angle of the attack and the sideslip angle are calculated as follows:

$$\alpha = \arctan\frac{w}{v} \tag{9}$$

$$\beta = \arcsin\frac{u}{v_m} \tag{10}$$

For a cruciform missile, these aerodynamic forces are calculated as follows [25]:

$$\begin{bmatrix} F_{Ax} \\ F_{Ay} \\ F_{Az} \end{bmatrix} = -qS \begin{bmatrix} C_{x_0} + C_{x_2}\left(\alpha^2 + \beta^2\right) \\ C_N\beta \\ C_N\alpha \end{bmatrix} \tag{11}$$

where S is the reference wing area, d is the reference chord line, and $q = 0.5\rho v_m^2$ is the dynamic pressure, $v_m = \sqrt{u^2 + v^2 + w^2}$ is the total missile velocity and ρ is the air density. Coefficients C_{x_0}, C_{x_2} and C_N are the aerodynamic coefficients measured at different angles of the attack, sideslip angles and Mach number. These numbers can be determined in a wind tunnel or using a specialized software, such as Missile DATCOM. For subsonic flights, these coefficients do not vary considerably. For a complete model, moments acting on the missile airframe need to be calculated. The aerodynamic forces act at the point termed the center of the pressure, while the missile rotates around its center of the gravity. These two points are displaced by distance r_x. The wing deflections and missile rotation also cause moments

which need to be calculated. The total moments are calculated as follows [25]:

$$\begin{bmatrix} L \\ M \\ N \end{bmatrix} = \begin{bmatrix} 0 \\ -r_X F_{AZ} \\ r_X F_{AY} \end{bmatrix} + \frac{qSd}{v_m} \begin{bmatrix} C_{LP}P \\ C_{MQ}Q \\ C_{NR}R \end{bmatrix} + qSd \begin{bmatrix} C_{L\delta_E}\delta_E \\ C_{M\delta_V}\delta_V \\ C_{N\delta_P}\delta_P \end{bmatrix} \tag{12}$$

where C_{LP}, C_{MQ} and C_{NR} are the aerodynamic stability coefficients, $C_{L\delta_E}$, $C_{M\delta_V}$ and $C_{N\delta_P}$ are the aerodynamic control coefficients and δ_E, δ_V and δ_P are the aileron, flaps and rudder deflections, respectively. To define the whole model, the transformation from the angular velocities to the derivatives of the Euler RPY angles is defined as follows:

$$\begin{bmatrix} \dot{\phi} \\ \dot{\theta} \\ \dot{\psi} \end{bmatrix} = \begin{bmatrix} 1 & \sin\phi\tan\theta & \cos\phi\tan\theta \\ 0 & \cos\phi & -\sin\phi \\ 0 & \frac{\sin\phi}{\cos\theta} & \frac{\cos\phi}{\cos\theta} \end{bmatrix} \begin{bmatrix} P \\ Q \\ R \end{bmatrix} \tag{13}$$

Finally, to simulate the missile position relative to the inertial frame, the velocities given in the inertial frame are transformed into the inertial frame as follows:

$$\begin{bmatrix} \dot{x}_m \\ \dot{y}_m \\ \dot{z}_m \end{bmatrix} = T_B^{E\,-1} \begin{bmatrix} u \\ v \\ w \end{bmatrix} \tag{14}$$

Table 1 shows the used missile parameters [26] for the simulation inside Matlab and Simulink.

I_x	I_y, I_z	m	C_{x_2}
$0.024\,\mathrm{kgm}^2$	$0.958\,\mathrm{kgm}^2$	$11.25\,\mathrm{kg}$	0.484
C_{x_0}	$C_{N\delta_P}$	$C_{M\delta_V}$	$C_{L\delta_E}$
2.04	0.0905	0.0905	0.0905
C_N	C_{MQ}, C_{NR}	d	C_{LP}
3.298	-10	$0.2286\,\mathrm{m}$	0.0905
T	r_x	ρ	S
$750\,\mathrm{N}$	$-0.119\,\mathrm{m}$	$1.225\,\mathrm{kg/m}^3$	$0.0314\,\mathrm{m}^2$

Table 1. Missile parameters.

3 ACTUATOR MODEL

The presented missile dynamic model has three system inputs, i.e. δ_E, δ_V and δ_P. The tactical missiles usually have four control surfaces given in the $\times$ or $+$ configuration as shown in Figure 1. The combined motion of the four control surfaces gives either the elevator, rudder or aileron control deflections. In the $+$ configuration, surfaces 1 and 3 rotating in the same direction give the rudder deflections. Similarly, surfaces 2 and 4 rotating in the same direction give the elevator deflections. If surfaces 2 and 4 have an independent servo mechanism, their rotation gives the aileron deflections. In the $\times$ configuration, the autopilot pitch and yaw axes are each $45°$ from the planes of the adjacent control surfaces [25]. This implies that each of the four control surfaces is deflected equally for the pitch and the yaw maneouvers.

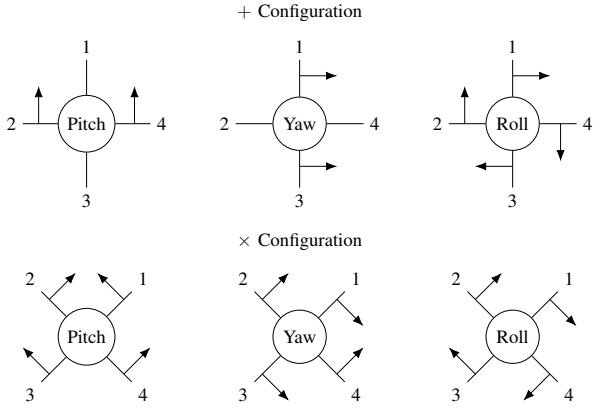

Figure 1. Missile wing configurations.

This means that the $\times$ configuration requires less surface deflections compared to the $+$ configuration. The autopilot calculates the elevator, rudder and aileron deflections. The computed deflections are transformed into four wing deflections using the transformation matrix given by the following expression:

$$\begin{bmatrix} \delta C_1 \\ \delta C_2 \\ \delta C_3 \\ \delta C_4 \end{bmatrix} = \begin{bmatrix} -1 & \cos\phi_P & -\sin\phi_P \\ -1 & \sin\phi_P & \cos\phi_P \\ 1 & \cos\phi_P & -\sin\phi_P \\ 1 & \sin\phi_P & \cos\phi_P \end{bmatrix} \begin{bmatrix} \delta P_{1C} \\ \delta P_{2C} \\ \delta P_{3C} \end{bmatrix} \tag{15}$$

where values δP_{1C}, δP_{2C} and δP_{3C} are the elevator, rudder and aileron commanding deflections calculated by the autopilot. Values δC_1, δC_2, δC_3 and δC_4 are the fin deflections required by each wing. The commanded fin deflections are usually limited. Angle ϕ_P is the angle by which the autopilot frame is rotated compared with the wings. For angle $\phi_P = 0$, the missile is in the $+$ configuration while angle $\phi_P = 45°$ yields the $\times$ configuration. The fins servomechanism ensures the fins to rotate for a commanded amount which yields real fin deflections δ_1, δ_2, δ_3 and δ_4. Fins are controlled by pneumatic, hydraulic, and electric actuators depending on the maximum required fin moment. The fin transfer function is modeled as a second order transfer function:

$$G_{Fin}(s) = \frac{\omega_n^2}{s^2 + 2\xi\omega_n s + \omega_n^2} \tag{16}$$

The fin servomechanism is implemented using a simple PID controller. The real fin deflections are then transformed back into the elevator, rudder and aileron deflections using the following transformation:

$$\begin{bmatrix} \delta_E \\ \delta_V \\ \delta_P \end{bmatrix} = \begin{bmatrix} -1/4 & -1/4 & 1/4 & 1/4 \\ 1/2 & 0 & 1/2 & 0 \\ 0 & 1/2 & 0 & 1/2 \end{bmatrix} \begin{bmatrix} \delta_1 \\ \delta_2 \\ \delta_3 \\ \delta_4 \end{bmatrix} \tag{17}$$

Using the transformations, the dynamic model is now more accurate since it takes into account also the saturation, dynamics and configuration of the actuators. The

maximum value of the control deflection is 30° and the tactical missiles are in the × configuration.

4 LATERAL ACCELERATION AUTOPILOT

The missile subsystem ensuring that the achieved missile accelerations are equal to the command accelerations by the guidance law is referred to as the autopilot. When roll angle ϕ is zero, there will be no cross-coupling between the pitch and yaw channels of the motion. This is achieved using a cascading PI controller with a measured roll angle in the feedback loop. The controller design is shown in Figure 2. The inner feedback loop is a damping loop which ensures minimal oscillations in the roll angle response. The outer loop ensures that the roll angle is always equal to zero. When the missile is stabilized in the roll channel, the pitch and the yaw movements are controlled independently. The main goal of the autopilot is to ensure that the missile lateral acceleration is equal to the commanded lateral acceleration for the vertical and horizontal guidance plane. Therefore, there is one controller for the vertical plane and one for the horizontal guidance plane. The two controllers have the structure given in Figure 2. The missile lateral

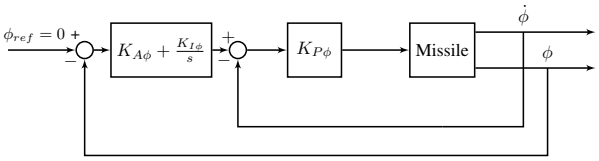

Figure 2. Roll controller design.

accelerations are given in the wind frame whose x axis is colinear with the wind direction. The derivative of the rotating velocity vector is given in the body frame. The velocity derivative is transformed into the wind body frame via the following transformation matrix:

$$T_B^W = \begin{bmatrix} \cos\alpha\cos\beta & \sin\beta & \sin\alpha\cos\beta \\ -\cos\alpha\sin\beta & \cos\beta & -\sin\alpha\sin\beta \\ -\sin\alpha & 0 & \cos\alpha \end{bmatrix} \quad (18)$$

The missile lateral accelerations are given by:

$$\begin{bmatrix} a_x \\ a_y \\ a_z \end{bmatrix} = T_B^W \left(\begin{bmatrix} \dot{u} \\ \dot{v} \\ \dot{w} \end{bmatrix} + \begin{bmatrix} P \\ Q \\ R \end{bmatrix} \times \begin{bmatrix} u \\ v \\ w \end{bmatrix} \right) \quad (19)$$

where a_y and a_z are the missile horizontal and lateral accelerations normal to the velocity vector in the wind frame and a_x is the acceleration along the velocity vector. Component a_x is usually equal to zero since the missile velocity does not change considerably during the terminal phase of the flight. Figure 3 shows the design of the lateral acceleration controller for the vertical guidance plane. The aerodynamic coefficients change with respect to the Mach number, angle of the attack, sideslip angle and other state variables. Therefore, it

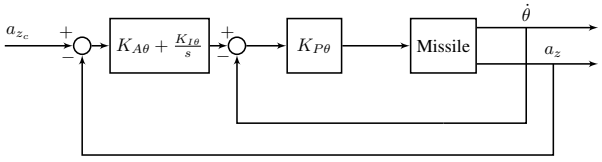

Figure 3. Lateral acceleration controller design.

is advisable to create multiple controllers for various operating points. The design approach is called the gain scheduling [27], [28]. Similarly at the subsonic flights, these aerodynamic coefficients do not vary much, so it is enough to design only one controller.

5 PN AND APN NAVIGATION

PN is perhaps the most used guidance law [29]. The task is to generate commanding accelerations that are proportional to the angular LOS rate. The commanding accelerations are calculated as follows:

$$a_{c_{PN}} = N\dot{\lambda}v_c \quad (20)$$

where a_c is the commanded lateral acceleration normal to the the line of sight, $N \geq 2$ is the effective navigational ratio and v_c is the closing velocity. The LOS angular rate is measured by the missile seeker as explained in Section VI. Ideally, the commanded lateral acceleration should be normal to LOS. However, most autopilots can control their accelerations normal to the missiles velocity vector. The PN variant whose commanding accelerations are normal to the velocity vector is known as a pure PN (PPN) [29]. If the target

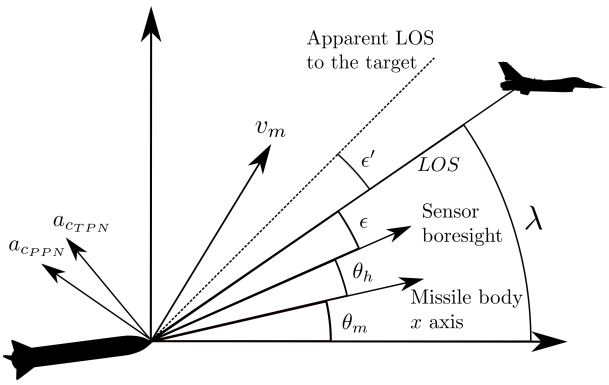

Figure 4. PN geometry.

is not maneuvering, the PN guidance law guarantees an interception of the target, provided that the lateral acceleration capability of the missile is not exceeded. As seen in Figure 4, LOS is calculated as:

$$\lambda = \arctan\frac{y}{r_x} \approx \arctan\frac{y}{r} = \frac{y}{v_c t_{go}} \quad (21)$$

where $r = v_c t_{go}$ is the range to the target, r_x is the horizontal range to the target, $t_{go} = t_f - t$ is the time

to go, t_f is the time of the interception and y is the vertical distance of the missile to the target. The LOS rate is given by:

$$\dot{\lambda} = \frac{y + \dot{y}t_{go}}{v_c t_{go}^2} \tag{22}$$

Therefore, the PN commanding acceleration can also be expressed as:

$$a_{c_{PN}} = N\frac{(y + \dot{y}t_{go})}{t_{go}^2}v_c \tag{23}$$

The expression in the parentheses of the preceding equation is termed the zero effort miss and it represents the future separation between the missile and the target if the missile makes no further lateral acceleration, assuming the target and missile continue with their current velocities. If the target is maneuvering, the zero effort miss is given by:

$$\text{ZEM} = y + \dot{y}t_{go} + \frac{1}{2}a_T t_{go}^2 \tag{24}$$

Therefore, a new guidance law can be defined as:

$$a_{c_{APN}} = N\dot{\lambda}v_c + \frac{1}{2}Na_T \tag{25}$$

and is referred to as the APN. Let us now consider the missile maneuvering characteristics when using the PN and APN guidance laws. In case of a maneuvering target, a 2D linearized engagement model is given by:

$$\ddot{y} = a_T - a_c \tag{26}$$

After using 23 in 26 and assuming $y(0) = \dot{y}(0) = 0$, the commanding lateral acceleration for the PN guidance is:

$$a_{c_{PN}} = \frac{Na_T}{N-2}\left(1 - \left(1 - \frac{t}{t_f}\right)^{N-2}\right) \tag{27}$$

In case of the APN guidance law, the commanding lateral acceleration is obtained by using 25 in 26:

$$a_{c_{APN}} = \frac{1}{2}Na_T\left(1 - \frac{t}{t_f}\right)^{N-2} \tag{28}$$

Figure 5 shows the commanding accelerations for the PN and APN guidance laws. As seen, the PN guidance law requires higher acceleration demands as the flight time increases. Also, it requires three times the acceleration of the target at the end of the flight for $N = 3$. On the other hand, the APN guidance law requires the maximum acceleration at the beginning of the flight which then decreases towards the end of the flight. This means that the APN guidance law is more anticipatory due to the fact that it requires the maximum acceleration at the beginning of the flight. Figure 5 also shows that for effective navigation ratio $N = 4$, the maximum required acceleration is the same and that the required acceleration is less for the APN guidance law by some 70% of the flight time. This can also be quantified by

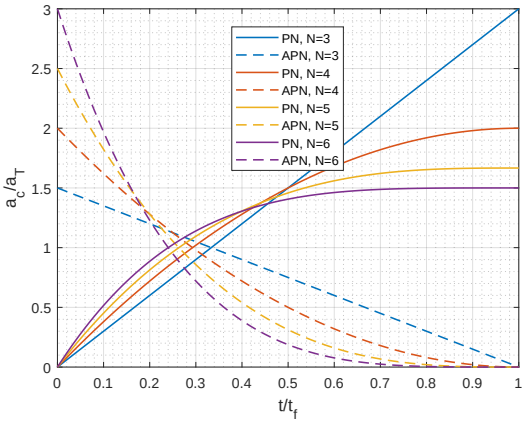

Figure 5. PN and APN commanding accelerations.

defining the performance index as the integral of the absolute value of the commanding acceleration over the flight time. The above confirms the fact that the APN guidance utilizes the information of the target acceleration. For the guidance in the three dimensions, the PN commanding accelerations are calculated as:

$$a_{c_{PN_y}} = N\dot{\lambda}_h v_c \tag{29}$$

$$a_{c_{PN_z}} = N\dot{\lambda}_v v_c \tag{30}$$

where $\dot{\lambda}_h$ and $\dot{\lambda}_v$ are the LOS rates in the horizontal and vertical plane respectively. Similarly, the APN commanding accelerations in three dimensions are calculated as:

$$a_{c_{APN_y}} = N\dot{\lambda}_h v_c + \frac{1}{2}Na_{T_h} \tag{31}$$

$$a_{c_{APN_z}} = N\dot{\lambda}_v v_c + \frac{1}{2}Na_{T_v} \tag{32}$$

where a_{T_h} and a_{T_v} are the target accelerations in the horizontal and vertical plane respectively.

6 YOLO

To track the target and calculate tracking errors ϵ_h and ϵ_v, the object needs to be localized in the image. The algorithm must then classify and localize the object in the obtained image. There are a handful of requirements that the localization algorithm has to satisfy in missile guidance applications. First, during simulations, images are obtained from an Unreal Engine environment, so the algorithm must be able to work with artificial images. Second, the algorithm has to be sufficiently fast since the camera can generate images at a high frequency. The most suitable localization algorithm in this case is the You Only Look Once (YOLO) convolutional neural network. YOLO was first introduced in 2016 when the object detection was reframed as a single regression problem straight from the image pixels to the bounding box and class probabilities [9]. This ensured that YOLO

needed only one passage through the network to obtain localization results, making it much faster than the existing algorithms which were based on region proposals. Over time, a number of object detectors based on YOLO have been developed. Most notably, YOLO9000 [30], YOLOv3 [31] and YOLOv4 [32] and YOLOv8 [33]. In our work we use the latest available YOLO implementation in Matlab pretrained on the Common Objects in Context (COCO) dataset [34] consisting of 80 classes and over 330000 images.

7 Camera Model

In the pinhole camera model shown in Figure 6, let X

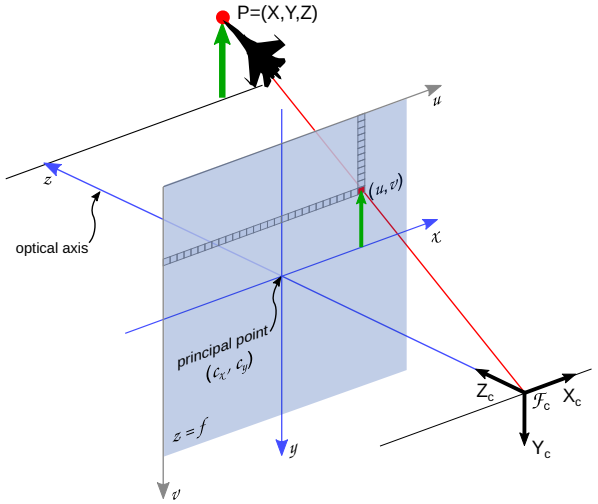

Figure 6. Pinhole camera model.

and Y denote the object size let u and v the size of the target image in the image plane in pixels. f_x and f_y denote the horizontal and the vertical focal length measured in pixels which is also the distance of the image plane from the CCD sensor. Figure 6 shows that the tracking error angle in the vertical plane is evaluated as follows:

$$\epsilon_v = \arctan \frac{v}{f_y} \tag{33}$$

For the horizontal tracking error angle, the equation is analogous:

$$\epsilon_h = \arctan \frac{u}{f_x} \tag{34}$$

It is simple now to calculate the tracking errors. The YOLO detector obtains the bounding box around the detected target with the coordinates of the upper left corner (denoted with x_t and y_t) and its width and height (denoted with w and h). Now the expressions for the vertical and horizontal tracking errors are:

$$\epsilon_v = \arctan \frac{y_t + h/2 - c_x}{f_x} \tag{35}$$

$$\epsilon_h = \arctan \frac{x_t + w/2 - c_y}{f_y} \tag{36}$$

where (c_x, c_y) is the principal point, $(c_x, c_y) = (0, 0)$, since the pixel coordinates are centered at the image center.

8 Gimbaled Seeker and LOS Rate Reconstruction

The seeker is an angular tracking device which can track LOS in the inertial space [18]. For the skid-to-turn missile, seekers can be classified as strapdown, semi-strapdown, stabilized platform-based and dynamic gyro stabilized seekers. In our paper, we consider dynamic gyro stabilized seekers which have two angular degrees of the freedom relative to the missile body. The camera is a detector mounted on the gimbaled system controlled by two DC motors rotating in the horizontal and vertical plane independently from the missile. Figure 7 shows the gimbal system for the missile seeker. Each gimbal DC

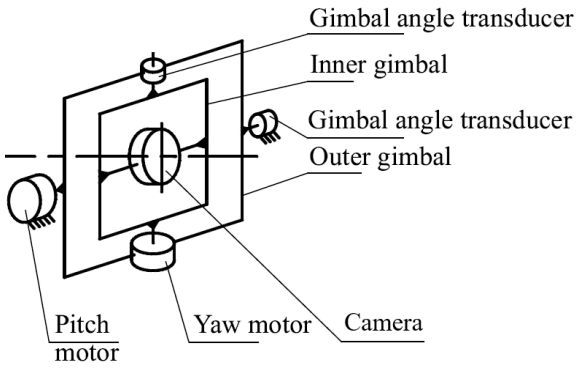

Figure 7. Gimbal system for the missile seeker.

motor is defined by its angular yaw position ψ_h or pitch position θ_h and angular yawing velocity $\dot{\psi}_h$ or pitching velocity $\dot{\theta}_h$. Each gimbal DC motor can be expressed by the open loop transfer function:

$$\frac{\Psi_h(s)}{U(s)} = \frac{\omega_n^2}{s\,(s + 2\xi\omega_n)} \tag{37}$$

$$\frac{\Theta_h(s)}{U(s)} = \frac{\omega_n^2}{s\,(s + 2\xi\omega_n)} \tag{38}$$

To minimize the radome refraction error [35], [36], the target should be kept in the center of the image. Therefore, the tracking errors are used as the error inputs to the controller driving the missile seeker. A standard PID controller [37]–[39] is used to control the seeker motors and to ensure that the tracking errors are minimized. As seen from the Figure 4, the LOS rate in the horizontal plane is measured as in [36], [40]:

$$\dot{\lambda}_{y_m} = \dot{\psi}_m + \dot{\psi}_h + \frac{s}{\tau_f s + 1}\,\epsilon_h \tag{39}$$

Similarly, the LOS rate in the vertical plane is given by

$$\dot{\lambda}_{z_m} = \dot{\theta}_m + \dot{\theta}_h + \frac{s}{\tau_f s + 1}\,\epsilon_v \tag{40}$$

where $\dot{\psi}_m$ and $\dot{\theta}_m$ are the missile yaw and thepitch rates, respectively, ϵ_h and ϵ_v are the horizontal and vertical tracking errors, and $\tau_f = 0.05\,\text{s}$ is the filter time constant.

9 EKF

The state of the target is not known a priori and must be estimated from the sensor measurements. EKF is perhaps the most widely used nonlinear estimator [41], [42]. However, it relies on local linearization of the nonlinear system dynamics and measurement model, which introduces approximation errors. As a result, its performance is generally suboptimal, especially in highly nonlinear scenarios. Nevertheless, it is employed here to recursively estimate the target state by fusing the measurements with the predicted state from the target model. Furthermore, the LOS rate and range measurements contain a noise which has to be filtered. EKF must provide accurate estimates of the LOS rates and the target acceleration in order to implement the PN and APN guidance laws. An effective guidance requires an estimator with a sufficient responsiveness, but an increased speed inevitably increases its sensitivity to the noise. These competing demands lead to an unavoidable trade-off. In order to implement EKF, a kinematic model is required. The guidance system disturbances are modeled as constant target lateral accelerations in the horizontal and vertical inertial planes denoted by a_{t_h} and a_{t_v}, respectively. Both acceleration components are defined in the plane orthogonal to the target's velocity vector. The total target velocity is assumed to be constant and equal to v_t. Let x_r, y_r and z_r denote the distance of the target to the missile in the inertial frame along the x, y and z axes, respectively. Let Θ_t and Ψ_t be the target velocity vectors azimuth and elevation angles, respectively. Equations governing the target orientations are given by:

$$\dot{\Psi}_t = \frac{a_{t_h}}{v_t \cos\Theta_t} \tag{41}$$

$$\dot{\Theta}_t = -\frac{a_{t_v}}{v_t} \tag{42}$$

$$\dot{a}_{t_h} = 0 \tag{43}$$

$$\dot{a}_{t_v} = 0 \tag{44}$$

with given initial orientations Ψ_{t_0} and Θ_{t_0}. The relative distance of the target from the missle in the inertial frame can now be defined by the following differential equations:

$$\dot{x}_r = v_t \cos\Theta_t \cos\Psi_t - v_m \cos\Theta_m \cos\Psi_m \tag{45}$$

$$\dot{y}_r = v_t \cos\Theta_t \sin\Psi_t - v_m \cos\Theta_m \sin\Psi_m \tag{46}$$

$$\dot{z}_r = -v_t \sin\Theta_t + v_m \sin\Theta_m \tag{47}$$

for given initial conditions x_{r_0}, y_{r_0} and z_{r_0}. The missile kinematic model is given by:

$$\dot{\Psi}_m = \frac{a_{m_h}}{v_m \cos\Theta_m} \tag{48}$$

$$\dot{\Theta}_m = -\frac{a_{m_v}}{v_m} \tag{49}$$

with some initial conditions Ψ_{m_0}, Θ_{m_0}. The inputs to the filter are missile velocity v_m and missile lateral accelerations a_{m_h} and a_{m_v}, which are accurately measured by the inertial measurement unit (IMU). Therefore, the EKF state vector is given by:

$$X = \begin{bmatrix} x_r & y_r & z_r & \Psi_m & \Theta_m \\ \Psi_t & \Theta_t & v_t & a_{t_h} & a_{t_v} \end{bmatrix}^T \tag{50}$$

The measurements are the range, missile velocity, and its lateral accelerations and the LOS rates obtained from the seeker. The range can be calculated as:

$$||\vec{R}|| = \sqrt{x_r^2 + y_r^2 + z_r^2} \tag{51}$$

In the three dimensions, the LOS rate can be expressed as:

$$\vec{\omega} = \frac{\vec{v}_c \times \vec{R}}{\left\|\vec{R}\right\|^2} \tag{52}$$

where $\vec{v}_c = \begin{bmatrix} \dot{x}_r & \dot{y}_r & \dot{z}_r \end{bmatrix}^T$ and $\vec{R} = \begin{bmatrix} x_r & y_r & z_r \end{bmatrix}^T$. Equations (45)–(47) and (51) can be substituted into (52), from which the LOS rates in the horizontal and vertical planes can be obtained as the second and third components of the LOS rate vector, respectively, as follows:

$$\dot{\lambda}_h = \frac{1}{r^2}[y_r \left(v_t \cos\Theta_t \cos\Psi_t - v_m \cos\Theta_m \cos\Psi_m\right) - x_r \left(v_t \cos\Theta_t \sin\Psi_t - v_m \cos\Theta_m \sin\Psi_m\right)] \tag{53}$$

$$\dot{\lambda}_v = \frac{1}{r^2}[x_r \left(v_m \sin\Theta_m - v_t \sin\Theta_t\right) - z_r \left(v_t \cos\Theta_t \cos\Psi_t - v_m \cos\Theta_m \cos\Psi_m\right)] \tag{54}$$

Now, the measurement vector can be defined as:

$$h(X) = \begin{bmatrix} r & \dot{\lambda}_h & \dot{\lambda}_v \end{bmatrix}^T \tag{55}$$

It is worth noting that the guidance system requires filtered LOS rates, so they have to be calculated from the measurement function using Equation 51. EKF is initialized using physically meaningful covariance values. Initial error covariance matrix P_0, process noise covariance matrix Q, and measurement noise covariance matrix R are selected according to realistic uncertainty bounds of the corresponding state variables and sensor measurements. The chosen values reflect the expected target maneuverability and sensor accuracy, and are tuned to ensure a stable and consistent filter convergence. The EKF algorithm and its implementation are well documented in [43], [44].

10 GUIDANCE SYSTEM DESIGN

The overall guidance system design is shown in Figure 8. The laser range finder provides the range measurement. The camera provides the YOLO detector with the target images acquired at a $60\,Hz$ frequency. The seeker calculates the tracking errors, stabilizes the platform and provides the LOS rate measurements for EKF. The inertial measurement unit (IMU) provides the missile body angular and linear velocities from which the Euler angles and their rates are obtained by sensor fusion. IMU also provides the missile lateral accelerations. The seeker gimbal angles are measured by appropriate angle transducers mounted on the gimbal axes. EKF estimates the target state including the target and the missile total velocity from which the closing velocity is calculated. The filter also estimates the target lateral accelerations and the LOS rates. The estimated target state is then used to calculate the PN or APN commanding accelerations. The autopilot now ensures that the missile lateral accelerations are equal to the commanded lateral accelerations.

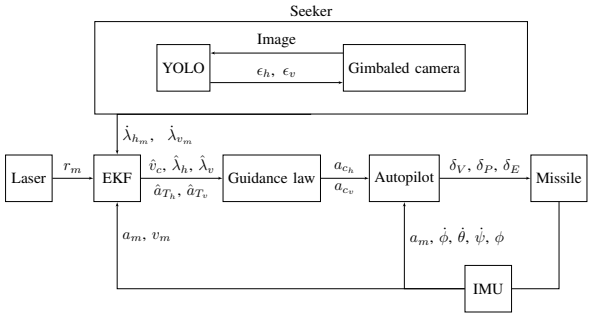

Figure 8. Missile guidance system design.

11 SIMULATIONS

Scenario 1: Consider a target at an initial distance of $500\,m$. The target is moving with a constant velocity of $80\,m/s$ and is accelerating with a constant lateral acceleration of $7\,m/s^2$ in the vertical plane and $-2\,m/s^2$ in the horizontal plane. Initial target and the missile orientations are $0\,rad$. The filter assumes that the target initial orientations are $\hat{\Psi}_t = \hat{\Theta}_t = 0.1\,rad$ and that the initial distance is $550\,m$. Figure 9 shows the missile and target trajectories. Figure 10 shows the tracking errors in the horizontal and vertical planes. It can be seen that the tracking errors converge to zero and the seeker is able to keep the target in the center of the image. Figure 11 shows the YOLO detection of the target in the camera image obtained from an Unreal Engine and Matlab cosimulation. It can be seen that YOLO is able to accurately detect and classify the target as an airplane. Figure 12 shows the estimated target lateral accelerations. It can be seen that the EKF is able

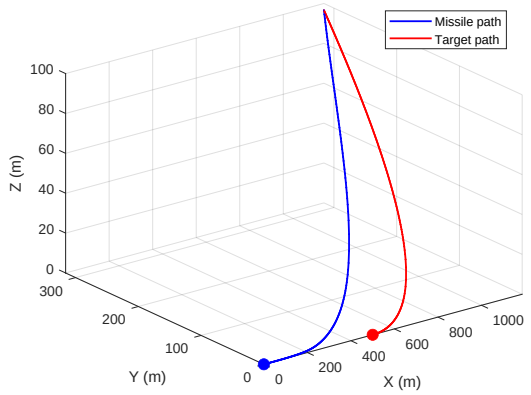

Figure 9. Missile and target trajectories.

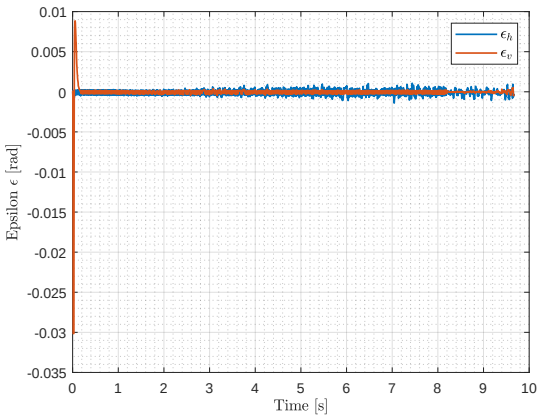

Figure 10. Tracking errors.

to accurately estimate the target accelerations. Figure 13 shows the estimated LOS rates in the horizontal and vertical planes. It can be seen the EKF accurately filters the measured LOS rates. Figure 14 shows the measured, estimated and real distance to the target. It is shown that EKF estimates the distance to the target despite the initial estimation error. The graph shows the estimated distance using Equation 51 since EKF does not directly

Figure 11. Classification and localization of an airplane.

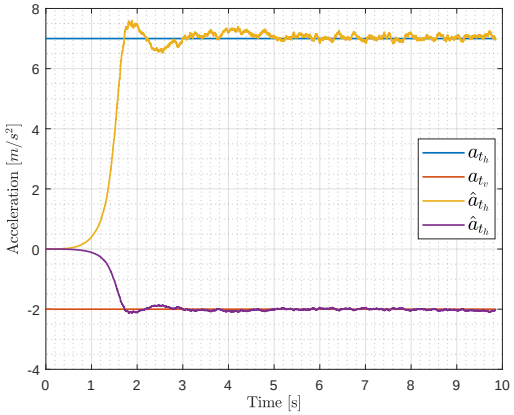

Figure 12. Estimated target horizontal and vertical lateral acceleration.

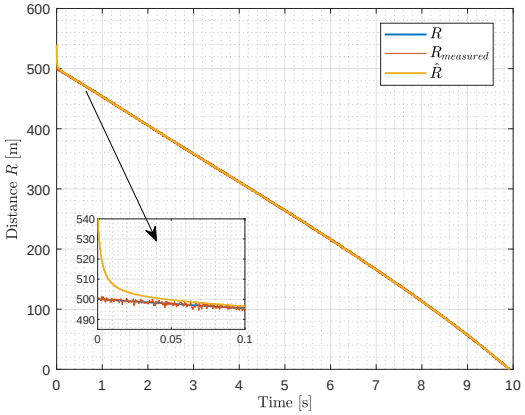

Figure 14. Measured, estimated and real distance.

estimate the distance. Figure 15 depicts the evolution of

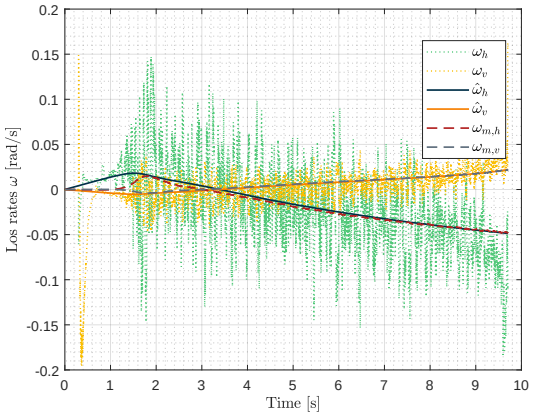

Figure 13. Estimated LOS rates.

the diagonal elements of EKF error covariance matrix P. The elements represent the estimation error variances associated with each state variable. It can be observed that all variances decrease and converge to small steady-state values, indicating that the filter uncertainty is reduced over time. This behavior confirms that EKF successfully incorporates the available measurements and provides consistent state estimates of the target. Figure 16 shows the commanded and achieved missile lateral accelerations for the PN and APN guidance laws when the effective navigation ratio is $N = 3$. It can be seen that the APN guidance law requires a smaller maximum and overall acceleration compared to the PN guidance law in the practical implementation with EKF. Figure 17 shows the integral of the absolute value of the missile lateral acceleration for both the PN and the APN guidance laws. This quantity, commonly referred to as the lateral divert, represents the total lateral control effort required during the engagement. It can be seen that, for most of the flight time, the APN guidance law requires

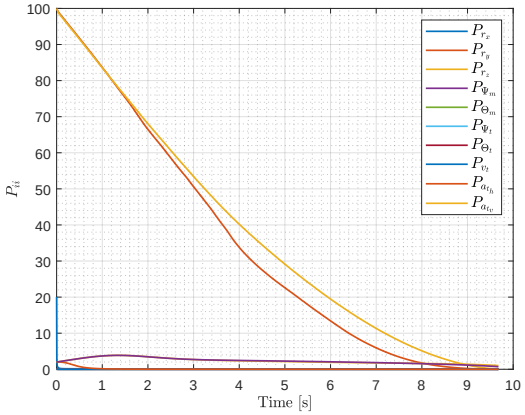

Figure 15. Estimated diagonal covariance.

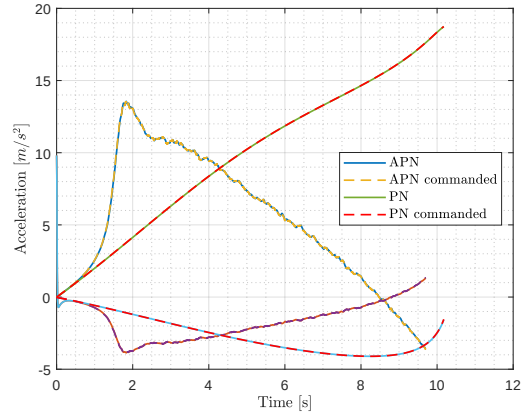

Figure 16. Commanded and achieved missile lateral accelerations for PN and APN guidance laws.

less lateral divert than PN, indicating that APN achieves the same intercept with a reduced lateral acceleration demand and therefore a higher guidance efficiency.

Scenario 2: In scenario 2, the target undergoes a constant lateral acceleration of 16 m/s^2 in the vertical plane

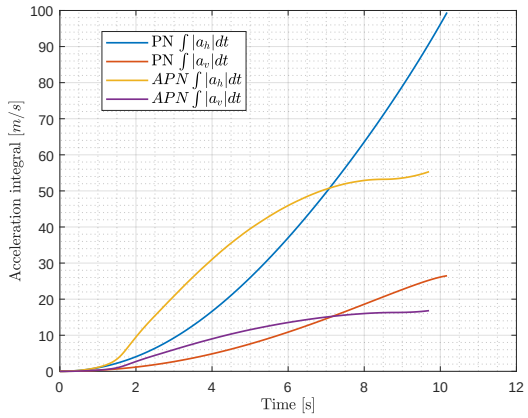

Figure 17. Integral of absolute value of the missile lateral acceleration for the PN and APN guidance laws.

and $-3\,\mathrm{m/s}^2$ in the horizontal plane. All other simulation parameters are identical to those used in Scenario 1. Since the wing deflections are limited to $30°$, the missile achievable lateral acceleration also reaches its saturation limit. It is important to note that the saturation limit depends on the full missile state vector and is therefore not constant across all flight conditions. For both guidance laws, EKF continues to accurately estimate the target lateral accelerations, as illustrated in Figure 18. In the

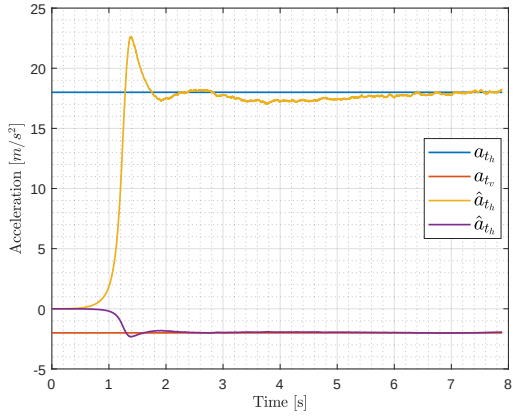

Figure 18. Estimated target accelerations for the scenario where the commanding acceleration exceeds the missile acceleration capability.

case of the APN guidance law, the missile is still able to intercept the target since the missile lateral acceleration capability is not exceeded as seen in Figure 19. It should be noted that the maximum acceleration should ideally be $a_{c_{APN_{\mathrm{MAX}}}} = a_T N/2 = 27\,m/s^2$. However, due to the EKF estimation overshoot, the resulting maximum commanding acceleration is $37.4\,m/s^2$. Despite the large maximum commanded acceleration, the missile is still able to intercept the target since the maximum commanded acceleration happens at the initial stage of the flight when the range to the target is large and the APN commanding acceleration decreases as the flight time increases. In contrast to the APN guidance law, for the PN guidance law, the missile is not able to intercept the target since its lateral acceleration capability is exceeded which leads to the final miss distance of $4.8\,m$. Furthermore, the PN commanding acceleration increases as the flight time increases as seen in Figure 20. This means that the missile lateral acceleration saturate at the end of the flight, thus making the miss more likely.

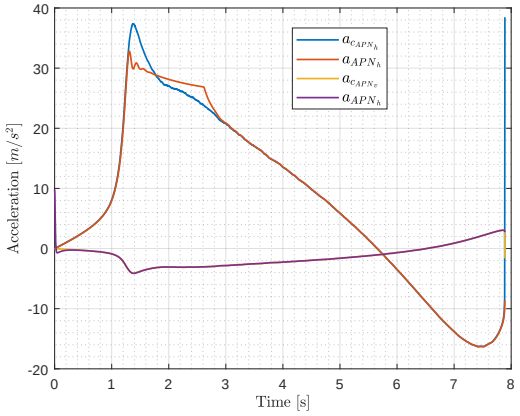

Figure 19. Commanded and achieved missile lateral accelerations for the APN guidance laws for scenario where the commanding acceleration exceeds the missile acceleration capability.

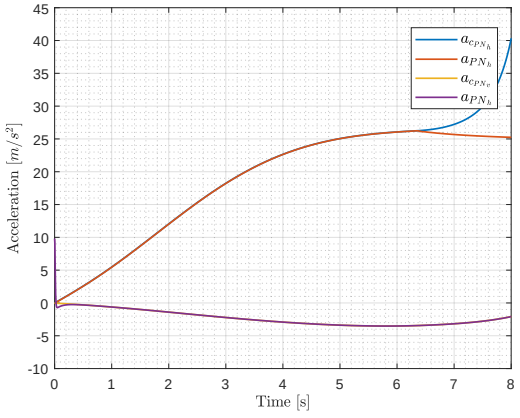

Figure 20. Commanded and achieved missile lateral accelerations for the PN guidance laws for the scenario where the commanding acceleration exceeds the missile acceleration capability.

12 Conclusion

The paper presents a design of a missile guidance system using the PN and APN guidance laws with an EKF to

estimate the target state vector. The gimbaled seeker with the YOLO object detector is used to track the target and to provide the LOS rate measurements to EKF together with a laser range finder. The simulation results show that the guidance system accurately estimates the target state and guides the missile towards the target. Furthermore, it is shown that the APN guidance law requires less maximum and overall missile lateral acceleration compared to the PN guidance law. The APN guidance law is therefore more likely to successfully intercept a highly maneuvering target compared to the PN guidance law since the commanding acceleration decreases as the flight time increases compared to the PN guidance law where the commanding acceleration increases as the flight time increases.

DATA AVAILABILITY STATEMENT

All the model parameters, system constants, and simulation settings required to reproduce the findings of our study are explicitly documented in the manuscript. The underlying MATLAB/Simulink source files (.slx and .m) are available from the corresponding author upon a reasonable request for verification and academic research purposes.

REFERENCES

[1] C.-D. Yang and C.-C. Yang, "A unified approach to proportional navigation," *"IEEE Transactions on Aerospace and Electronic Systems"*, vol. 33, no. 2, pp. 557–567, 1997.

[2] S. A. Murtaugh and H. E. Criel, "Fundamentals of proportional navigation," *"IEEE Spectrum"*, vol. 3, no. 12, pp. 75–85, 1966.

[3] M. Guelman, "A qualitative study of proportional navigation," *IEEE Transactions on Aerospace and Electronic Systems*, vol. AES-7, no. 4, pp. 637–643, 1971.

[4] ——, "Proportional navigation with a maneuvering target," *"IEEE Transactions on Aerospace and Electronic Systems"*, vol. AES-8, no. 3, pp. 364–371, 1972.

[5] M. Abd-elatif, L. jun Qian, and Y. ming Bo, "Optimization of three-loop missile autopilot gain under crossover frequency constraint," *"Defence Technology"*, vol. 12, no. 1, pp. 32–38, 2016.

[6] B. Zhang, Q. Lv, and Y. Lei, "The application of pid controller in missile longitudinal loop system and its simulation," in *Proceedings of the 5th International Conference on Advanced Design and Manufacturing Engineering*. Atlantis Press, 2015/10, pp. 2113–2118. [Online]. Available: https://doi.org/10.2991/icadme-15.2015.395

[7] A. Awad and H. Wang, "Roll-pitch-yaw autopilot design for nonlinear time-varying missile using partial state observer based global fast terminal sliding mode control," *"Chinese Journal of Aeronautics"*, vol. 29, no. 5, pp. 1302–1312, 2016. [Online]. Available: https://www.sciencedirect.com/science/article/pii/S1000936116301108

[8] L. Bruyere, A. Tsourdos, and B. A. White, "Quasilinear parameter-varying autopilot design using polynomial eigenstructure assignment with actuator constraints," *Journal of Guidance, Control, and Dynamics*, vol. 29, no. 6, pp. 1282–1294, 2006. [Online]. Available: https://doi.org/10.2514/1.17039

[9] J. Redmon, S. Divvala, R. Girshick, and A. Farhadi, "You only look once: Unified, real-time object detection," *https://arxiv.org/abs/1506.02640*, 2016.

[10] M. Hodžić and N. Prljača, "Missile guidance using proportional navigation and machine learning," *Journal of Engineering Research and Sciences*, vol. 3, pp. 19–26, 2024. [Online]. Available: https://dx.doi.org/10.55708/js0303003

[11] B. Boberg, J. Lundberg, J. Wiberg, and S.-L. Wirkander, "Estimation of target lateral acceleration for augmented proportional navigation," 08 1997.

[12] Y. Oshman and D. Arad, "Enhanced air-to-air missile tracking using target orientation observations," *Journal of Guidance Control and Dynamics - J GUID CONTROL DYNAM*, vol. 27, pp. 595–606, 07 2004.

[13] S. Pan, H. Su, J. Chu, and H. Wang, "Applying a novel extended kalman filter to missile–target interception with apn guidance law: A benchmark case study," *Control Engineering Practice*, vol. 18, no. 2, pp. 159–167, 2010, special Issue of the 3rd International Symposium on Advanced Control of Industrial Processes. [Online]. Available: https://www.sciencedirect.com/science/article/pii/S096706610900183X

[14] S. Niazi, "Estimation of los rates for target tracking problems using ekf and ukf algorithms- a comparative study," *International Journal of Engineering*, vol. 28, no. 2, pp. 172–179, 2015.

[15] D. S. R. Kondru, "Estimation of line-of-sight rate in a homing missile guidance loop using optimal filters," 04 2015.

[16] M. Liberato, E. Pizzingrilli, and S. Longhi, "Ekf application on estimating missile guidance signals," *Communications to SIMAI Congress*, vol. Vol. 3, p. 323 (9pp), 01 2009.

[17] J. Waldmann, "Line-of-sight rate estimation and linearizing control of an imaging seeker in a tactical missile guided by proportional navigation," *IEEE Transactions on Control Systems Technology*, vol. 10, no. 4, pp. 556–567, 2002.

[18] Q. Zaikang and L. Defu, *Design of Guidance and Control Systems for Tactical Missiles*, 1st ed. CRC Press, 2019.

[19] R. Yanushevsky, *Modern Missile Guidance*. Taylor & Francis, 2007.

[20] M. Drela, *Flight Vehicle Aerodynamics*, ser. FLIGHT VEHICLE AERODYNAMICS. MIT Press, 2014.

[21] S. Graovac, *Automatsko vođenje objekata u prostoru*. Akademska Misao, 2005.

[22] C.-F. Lin, *Modern Navigation, Guidance and Control Processing*. Prentice Hall, 1991.

[23] M. V. Cook, Ed., *Flight Dynamics Principles (Third Edition)*, third edition ed. Butterworth-Heinemann, 2013.

[24] M. Hodžić and N. Prljača, "Simulation of short range missile guidance using proportional navigation," in *2021 20th International Symposium INFOTEH-JAHORINA (INFOTEH)*, 2021, pp. 1–6.

[25] G. M. Siouris, *Missile Guidance and Control Systems*. Springer-Verlag New York, 2004.

[26] J. Harris and N. Slegers, "Performance of a fire-and-forget anti-tank missile with a damaged wing," *Mathematical and Computer Modelling*, vol. 50, no. 1, pp. 292–305, 2009.

[27] A. Hiret, G. Duc, and J. Bonnet, "The application of gain-scheduling h controllers for a missile autopilot," *"IFAC Proceedings Volumes"*, vol. 31, no. 21, pp. 59–64, 1998, 14th IFAC Symposium on Automatic Control in Aerospace 1998, Seoul, Korea, 24-28 August 1998. [Online]. Available: https://www.sciencedirect.com/science/article/pii/S1474667017410597

[28] D. White, J. Wozniak, and D. Lawrence, "Missile autopilot design using a gain scheduling technique," in *Proceedings of 26th Southeastern Symposium on System Theory*, 1994, pp. 606–610.

[29] U. Shukla and P. Mahapatra, "The proportional navigation dilemma-pure or true?" *"IEEE Transactions on Aerospace and Electronic Systems"*, vol. 26, no. 2, pp. 382–392, 1990.

[30] J. Redmon and A. Farhadi, "Yolo9000: Better, faster, stronger," *https://arxiv.org/abs/1612.08242*, 2016.

[31] ——, "Yolov3: An incremental improvement," *https://arxiv.org/abs/1804.02767*, 2018.

[32] A. Bochkovskiy, C.-Y. Wang, and H.-Y. M. Liao, "Yolov4: Optimal speed and accuracy of object detection," *https://arxiv.org/abs/2004.10934*, 2020.

[33] D. Reis, J. Kupec, J. Hong, and A. Daoudi, "Real-time flying object detection with yolov8," 2023.

[34] T.-Y. Lin, M. Maire, S. Belongie, L. Bourdev, R. Girshick, J. Hays, P. Perona, D. Ramanan, C. L. Zitnick, and P. Dollár, "Microsoft coco: Common objects in context," *https://arxiv.org/abs/1405.0312*, 2015.

[35] N. F. Palumbo, R. A. Blauwkamp, and J. M. Lloyd, "Basic principles of homing guidance," *Johns Hopkins Apl Technical Digest*, vol. 29, pp. 25–41, 2010. [Online]. Available: https://api.semanticscholar.org/CorpusID:1858151

[36] M. Hodžić and N. Prljača, "Los rate estimation techniques for proportional navigation guided missiles," in *2022 21st International Symposium INFOTEH-JAHORINA (INFOTEH)*, 2022, pp. 1–6.

[37] M. Sahin, "Gimbal axes control with pid controllers," *Gazi Üniversitesi Fen Bilimleri Dergisi Part C: Tasarım ve Teknoloji*, vol. 11, 02 2023.

[38] M. Abdo, A. R. Vali, A. R. Toloei, and M. R. Arvan, "Modeling control and simulation of two axes gimbal seeker using fuzzy pid controller," in *2014 22nd Iranian Conference on Electrical Engineering (ICEE)*, 2014, pp. 1342–1347.

[39] Q. Huang, J. Zhou, X. Chen, Y. Yao, Y. Chen, W. Chen, R. Chen, and Z. Lv, "Modeling and control of a two-axis stabilized gimbal based on kane method," *Sensors*, vol. 24, no. 11, p. 3615, 2024. [Online]. Available: https://doi.org/10.3390/s24113615

[40] F. W. Nesline and P. Zarchan, "Line-of-sight reconstruction for faster homing guidance," *Journal of Guidance Control and Dynamics*, vol. 8, pp. 3–8, 1985. [Online]. Available: https://api.semanticscholar.org/CorpusID:123234458

[41] P. S. Maybeck, *Stochastic Models: Estimation and Control*, ser. Mathematics in Science and Engineering. Academic Press, 1979. [Online]. Available: https://books.google.ba/books?id=FkkZBqQG36gC

[42] B. Anderson and J. Moore, *Optimal Filtering*. Prentice-Hall, 1979.

[43] D. Simon, *Optimal State Estimation: Kalman, H Infinity, and Nonlinear Approaches*. Hoboken, NJ: John Wiley & Sons, 2006.

[44] R. G. Brown and P. Y. C. Hwang, *Introduction to Random Signals and Applied Kalman Filtering*, 4th ed. Hoboken, NJ: John Wiley & Sons, 2012.

Mirza Hodžić recieved his B.Sc. and M.Sc. degrees in 2020 and 2022 respectively from the Faculty of Electrical Engineering Tuzla, Bosnia and Herzegovina. He works in the industry and at the Faculty of Electrical Engineering at the Department of Control Systems, Robotics and Industrial Informatics. His research interests are in robotics, control systems, machine vision and missile guidance. Currently, he is working towards his PhD degree in the field of control systems at the same faculty.

Naser Prljača is Full professor and Head of Department of Control Systems, Robotics and Industrial Informatics at the Faculty of Electrical Engineering, University of Tuzla, Bosnia and Herzegovina. He holds the B.Sc., M.Sc. and Ph.D. degrees in Electrical and Electronics Engineering. He has been taking part in numerous research and industrial projects, and is an author of a number of academic publications. His research and teaching interests include control systems, embedded systems, robotics, machine learning and computer vision.